



Article

Improvement in the Hard Milling of AISI D2 Steel under the MQCL Condition Using Emulsion-Dispersed MoS₂ Nanosheets

Pham Quang Dong ¹, Tran Minh Duc ¹, Ngo Minh Tuan ¹, Tran The Long ^{1,*} , Dang Van Thanh ² and Nguyen Van Truong ³

- ¹ Department of Manufacturing Engineering, Faculty of Mechanical Engineering, Thai Nguyen University of Technology, Thai Nguyen 250000, Vietnam; quangdongctm@tnut.edu.vn (P.Q.D.); minhduc@tnut.edu.vn (T.M.D.); minhtuanngo@tnut.edu.vn (N.M.T.)
- ² Faculty of Basic Sciences, College of Medicine and Pharmacy, Thai Nguyen University, Thai Nguyen 250000, Vietnam; thanhdv@tnmc.edu.vn
- ³ Faculty of Fundamental of Sciences, Thai Nguyen University of Technology, Thai Nguyen 250000, Vietnam; truonglyk3@gmail.com
- * Correspondence: tranthelong90@gmail.com or tranthelong@tnut.edu.vn; Tel.: +84-985-288-777

Received: 9 May 2020; Accepted: 1 June 2020; Published: 5 June 2020



Abstract: The present work shows the process for MoS₂ nanosheet production by liquid N₂-quenched bulk, a novel method having highly efficient, green, and facile operation. The produced MoS₂ nanoparticles are suspended in minimum quantity cooling lubrication (MQCL)-based fluid to form nanofluid used for the hard milling of AISI D2 steel. The study aims to improve the hard-milling performance assisted by the MQCL technique using MoS₂ nanofluid. ANOVA analysis is used to evaluate the effects of three input machining variables, including nanoparticle concentration, cutting speed, and material hardness on cutting forces. The results indicate that the better cooling effect from the principle of the Ranque–Hilsch vortex tube of the MQCL device combined with the better lubricating performance from MoS₂ nanofluid brings out the sustainable alternative solution for machining difficult-to-cut material. Moreover, the experimental results provide the technical guides for the selection of proper values of nanoparticle concentration and cutting speed while ensuring the technological, economic, and environmental characteristics.

Keywords: liquid N₂-quenched bulk; hard milling; MQCL; MoS₂ nanosheets; nanofluid; cutting force; difficult-to-cut material

1. Introduction

In the machining field, the manufacture of difficult-to-cut materials, especially hardened steel, has been growing concern not only for researchers but also for manufacturers around the world. Hardened steels have been widely used in different applications, such as mold and die, automotive components, bearings, and so on. They possess high hardness and strength properties, which makes them difficult to cut by using the conventional machining processes like turning, milling, and drilling due to large cutting forces, high cutting temperature, and severe tool wear. Traditionally, grinding operations have been the most common in machining hardened steel components (45–65 HRC). However, the low productivity, high cost, and environmental issues caused by cutting fluids are considered the main drawbacks of the grinding process [1]. Accordingly, the hard machining processes, such as hard turning, milling and drilling, have been developed to meet the growing demand of high productivity, good surface quality, coolant elimination, manufacturing cost reduction, and flexibility to different types of parts [2]. Hard turning was early recognized and applied in the automotive

industry, which proved the effectiveness in technological, economic, and environmental characteristics in machining the transmission components when compared to grinding. In addition, a typical example of early applications of hard turning is the surface of gear-wheel bearings by using polycrystalline cubic boron nitride (CBN) inserts. Nevertheless, the enormous cutting heat and large cutting forces are always the main problems when applying hard machining processes, which require the high-graded inserts like coated cemented carbide, ceramics, (Polycrystalline) Cubic Boron Nitride ((P)CBN), Polycrystalline Diamond (PCD) tools [3–6]. Furthermore, dry hard cutting is often used to avoid thermal shock leading to tool failure and retain the environmentally friendly character. This also limits the range of cutting conditions and the productivity as well as the increase of manufacturing cost. Therefore, the alternative solutions have been studied and proposed to improve the cutting performance of hard machining processes, including non-traditional cutting processes assisted in machining, such as laser-assisted machining (LAM) [7,8], minimum quantity lubrication (MQL) and minimum quantity cooling lubrication (MQCL) assisted in machining and nanofluids enriched in MQL and MQCL-assisted machining [9–17]. Among these novel approaches, the utilization of nano additives suspended in MQL- and MQCL-based fluids was proven the significant improvement in hard cutting performance. B. Li and his co-authors (2017) [18] investigated the performance of the heat transfer of different types of nanoparticles (MoS_2 , ZrO_2 , CNT, PCD, Al_2O_3 , SiO_2) enriched in MQL-based fluid in the grinding process of Ni-based alloy. The authors pointed out that the viscosity and thermal conductivity of MQL-based fluid improved by suspending nanoparticles, from which grinding forces and heat significantly decreased. F. Pashmforoush et al. (2018) [19] also made the study on the grinding process of Inconel 738 super alloy by using dry condition, conventional fluid and CuO nanofluid. The values of the wheel loading ratio and surface roughness decreased when compared to dry grinding and conventional fluid grinding. The nanoparticles' concentration and feed velocity have strong effects on surface roughness and wheel loading. Pil-Ho Lee et al. (2012) [20] studied the diamond and Al_2O_3 NFMQL (nanofluid minimum quantity lubrication) performance in micro grinding. The authors concluded that the nano additives contribute to reduce grinding forces significantly and enhance the surface quality, especially in the case of using higher nanoparticles concentration and smaller grain size. Y. Zhang et al. (2016) [21] had done the study on mass volume of nanoparticles MoS_2 and CNTs (carbon nanotubes) in MQL-based fluid in grinding process of Ni-based alloy. The lubrication performance improved and contributed to the better surface quality. Furthermore, the authors also investigated hybrid MoS_2 -CNTs nanofluid and made the comparison to the nanofluid with only one nanoparticle type. The obtained results indicated that the surface quality is better by using hybrid MoS_2 -CNTs nanofluid. On the other hand, there have been many studies on the NFMQL machining processes of difficult-to-cut materials using geometrical-defined cutting edges like turning, milling, and drilling. Ç. V. Yıldırım et al. (2019) [22] studied the effect of hBN nanofluid-MQL on tool wear, tool life, surface roughness and cutting temperature in the turning of Ni-based Inconel 625. The obtained results indicated that the tool life was considerably prolonged under NFMQL with 0.5 vol% hBN when compared to dry and pure MQL machining. The main reason for this is that the presence of hBN nanoparticles in oil mist enhances the cooling and lubricating effects, so the cutting forces and cutting temperature reduce, which decreases tool wear. In addition, the hBN ratio in coolant is a very important factor, which strongly influences the machining performance. In 2020, the author newly made the investigation of Cryogenic cooling by liquid nitrogen and NFMQL used in the hard turning of AISI 420 [23]. He concluded that the surface quality under NFMQL is better, while machining outputs in term of cutting temperature, tool life, tool wear, and chip morphology under cryogenic cooling show better results. The main reason for this observation is the superior cooling performance of liquid nitrogen compared to NFMQL, especially at high cutting speed. Another promising approach is the use of minimum quantity cooling lubrication (MQCL), which is the development of the MQL method to improve the cooling effect. This technique has been gaining growing attention for machining difficult-to-cut materials. S. Pervaiz et al. (2017) [24] investigated the turning process of Ti alloy under MQCL condition compared to dry and flood cutting. The better cooling and lubricating performance

is reported and contributes to reducing the friction coefficient in cutting zone, leading to the decrease in cutting forces and tool wear as well as the enhancement of surface quality. R. W. Maruda et al. (2017) [25] had done the investigation on hard turning of AISI 1045 steel under MQCL condition with emulsion fluid. The results revealed that the oil mist formed in cutting zone contributes to improve cooling and lubricating effects. The authors also investigated the formation of droplets and the relationship between the MQCL parameters and diameter [26]. In another study, they concluded that the chip shape is favorable and the decrease of the chip thickening coefficient is reported under MQCL condition due to better cooling and lubricating effectiveness [27]. The quadratic effects of MQCL parameters and droplets are also studied to bring out the possibility to choose the suitable condition for oil mist formation on the newly machined surface within 1 s and then evaporate [28]. However, the cooling effect of the MQCL methods used by the mentioned studies is based on the cutting fluid like emulsion, which already possesses the cooling and lubricating properties. The application of the MQCL technique with the real cooling effect is definitely the novel approach to improve the machining performance and enlarge MQCL applicability as well as to bring out the new alternative solutions for difficult-to-cut materials. Furthermore, MQCL using nanofluid is an up-to-date topic and is needed to study [17,29].

Among the common types of nanoparticles, molybdenum disulfide (MoS_2) possesses a low friction coefficient and excellent physical properties. This kind of nanoparticle also has a large active surface area, high reactivity, and increased adsorption capacity compared to the bulk material. Hence, MoS_2 nanofluid is found to be advantageous for improving the lubricating effect for machining processes. Several approaches have been proposed for producing MoS_2 nanosheet, including liquid exfoliation [30], chemical vapor deposition [31], thermal decomposition [32], the sulfurization of an Mo-based compound [33] and vapor–solid growth [34]. For instance, Zhang et al. [30] reported a fast and highly controllable approach to yield a variety of semiconducting nanosheets by exfoliation. Taking the benefit of the electrochemical lithiation discharge process, bulk MoS_2 could be intercalated by lithium ion and then a high-yield (92%), single-layer MoS_2 was achieved after subsequent ultrasonication. Ku et al. [32] successfully prepared a bi- and tri-layer of MoS_2 nanosheets by simple thermolysis of $(\text{NH}_4)_2\text{SO}_4$ at specific temperature. D.V. Thanh and our group [35] presented a novel and facile method by the exfoliation of liquid N_2 -quenched bulk MoS_2 . This technique is promising for further application owing to its highly efficient, green, and facile operation. The produced MoS_2 nanoparticles are suspended in MQCL-based fluid to form MoS_2 nanofluid used for the hard milling of AISI D2 steel. This paper aims to improve the cutting performance of the hard-milling process by applying novel cooling and lubricating method, nanofluid minimum quantity cooling lubrication (NFMQCL). The results indicate the promising alternative solution for machining difficult-to-cut materials while retaining the environmentally friendly characteristics, suitable for sustainable production.

2. Materials and Methods

2.1. The Production of MoS_2 Nanoparticles

The preparation of MoS_2 nanosheets by liquid N_2 -quenched bulk MoS_2 was reported in [35]. Briefly, 500 mg of MoS_2 bulk was transferred to 100 mL of 5% KOH solution under vigorous stirring for 30 min. The mixture was maintained at 80 °C for 24 h and then it was quickly quenched in liquid N_2 . The temperature dramatically dropped from 80 to –196 °C when the MoS_2 solution was immersed in liquid N_2 . This prompt temperature decreasing not only expands the MoS_2 but also allows for the intercalation of both K^+ ions and N_2 gas into the interlayer, resulting in exfoliating MoS_2 nanosheets under the sonication synergistic. After quenching, the dispersion was sonicated at 20 kHz under a power of 400 W. The resulting material was collected through vacuum filtration with PVDF membranes (average pore size: 0.2 μm). The final product was dried in 50 °C under vacuum for 24 h. The Raman spectra of bulk MoS_2 and MoS_2 nanosheets powders were recorded using a Raman Spectrometer JobinYvon LabRAM HR800 (FOCAS Research Institute, Dublin, Ireland).

Transmission electron microscopy (TEM) images were recorded using a JEM-2100F Field Emission Electron Microscope (JEOL Ltd., Tokyo, Japan).

Figure 1 displays the transmission electron microscopy (TEM) image, scanning electron microscopy (SEM) image, lateral size distribution and Raman spectra of MoS₂ flake obtained from the N₂-quenched exfoliation method [35]. A transparent to the electron beam corresponding to the sheet-like structures of MoS₂ flakes with a lateral size of approximately several hundred nanometers was shown in Figure 1a and the thickness ranges from 10 to 20 nm. Figure 1b displays the SEM image of MoS₂ flakes which clearly show the sheets morphology with the lateral size from several hundred nm to approximate 2 μm . Furthermore, a statistic was estimated from 75 objects in SEM images to evaluate the lateral size distribution of MoS₂ nanosheets as shown in Figure 1c. MoS₂ nanosheets almost reveal the lateral size smaller than 1 μm , which is consistent with the TEM data. In addition, the Raman spectra in Figure 1d reveal a typical of in-plane E¹_{2g} and out-plane A_{1g} Raman peaks of MoS₂ flakes located at 376 and 403.2 cm^{-1} , respectively, which highly agreed with the previous reports [36,37].

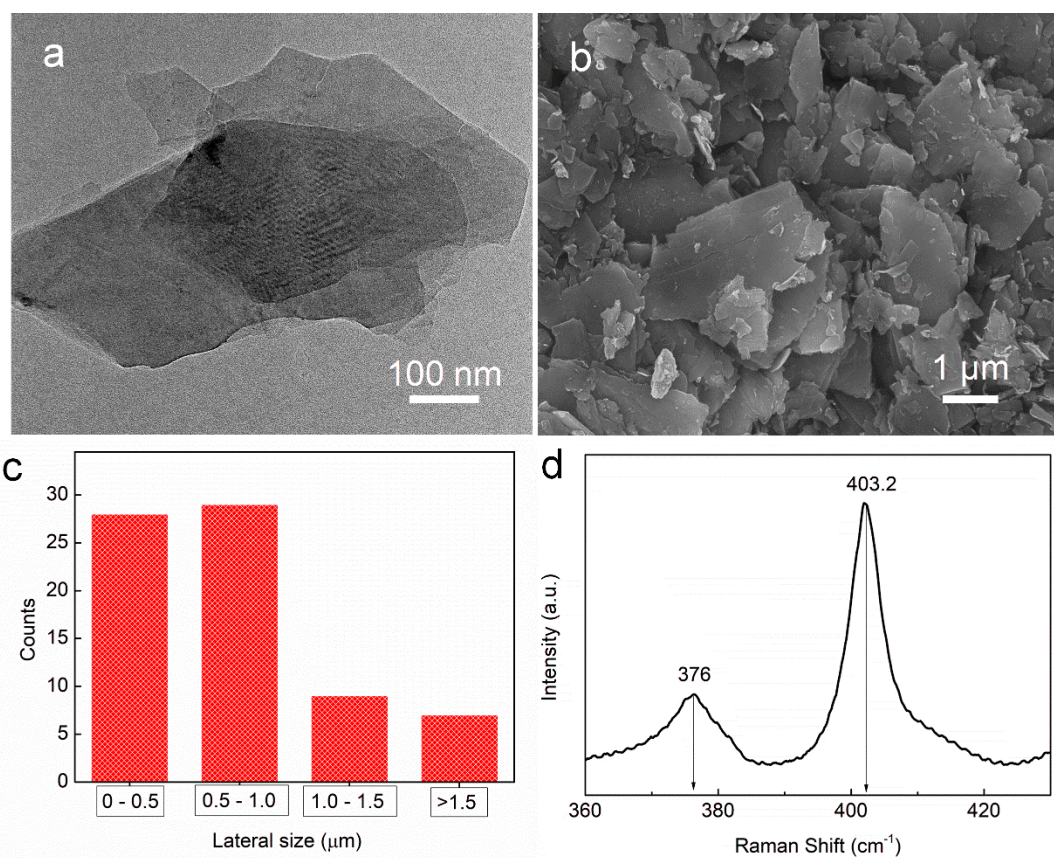


Figure 1. (a) Transmission electron microscopy (TEM) image, (b) scanning electron microscopy (SEM) image, (c) Lateral size distribution and Raman spectra (d) of MoS₂ nanosheets.

2.2. Experimental Set Up

The experimental devices consist of Mazak vertical center smart 530C (Yamazaki Mazak Corporation, Aichi, Japan), tool holder type with the designation SHIJIE BAP 400R-50-22-4T with the diameter of 50 mm, and APMT 1604 PDTR LT30 PVD submicron carbide inserts (LAMINA TECHNOLOGIES SA, Yverdons-les-Bains, Switzerland) with a flank angle of 11°, nose radius of 0.66 mm, and a TiAlN coating layer. The samples are AISI D2 steels (52–60 HRC) with the dimensions of 90 mm × 48 mm × 50 mm and their chemical composition shown in Table 1.

Table 1. Chemical composition of AISI D2 steel (According to American Society for Testing and Materials (ASTM) A681).

Chemical Composition (%)										
C	Si	Mn	Ni	Cr	Mo	W	V	P	S	
1.4–1.6	0.1–0.6	0.1–0.6	0.5	11.0–13.0	0.7–1.2	0.2–0.5	0.5–1.1	0.03	0.03	

The MQCL system includes Frigid-X Sub-Zero Vortex Tool Cooling Mist System (Nex Flow™ Air Products Corp, Richmond Hill, ON, Canada) compressed air, pressure stabilization device, water-based emulsion 5% and MoS₂ nanoparticles. The experiment set up is shown in Figure 2.

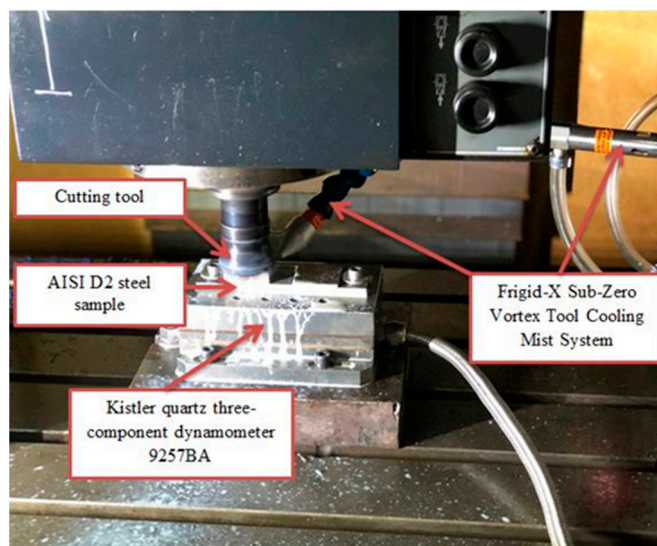


Figure 2. Experimental set up.

To ensure the uniform suspension of MoS₂ nanosheets in emulsion-based fluids, the prepared nanofluids are kept in Ultrasons-HD ultrasonicator (JP Selecta, Abrera (Barcelona), Spain), generating 400 W ultrasonic pulses at 40 kHz for 2 h to ensure the uniform distribution of the nanoparticles. In order to use the obtained nanofluids effectively and avoid the precipitation of agglomerated nanoparticles during the long time of machining, the nanofluid was placed in the 3000868-Ultrasons-HD and directly used for the MQCL system.

Measuring equipment consists of Kistler quartz three-component dynamometer 9257BA (Kistler Instruments (Pte) Ltd., Midview, Singapore).

2.3. Experiment Design

The fixed parameters for cutting condition include the feed rate of 0.012 mm/tooth, a depth of cut of 0.12 mm, air pressure of 0.6 MPa, flow rate of 30 mL/h; the room temperature 24–27 °C; the temperature of output cool air through MQCL nozzle of 4–8 °C. Box–Behnken experimental design is made with the help of Minitab 18.0 software (N03-T5 Embassy Garden, Ha Noi, Vietnam) (Table 2). Table A1 summarizes the design of experiment with test run order and output in term of cutting forces F_x, F_y, F_z. Each test run is repeated by three times under the same cutting parameters.

Table 2. Control factors and their levels.

Control Factor	Unit	Symbol	Level	
			Low	High
Nanoparticle concentration (np)	wt.%	x_1	0.5	1.5
Cutting speed (V)	m/min	x_2	90	110
Hardness	HRC	x_3	52	60

3. Results and Discussion

The Effects of Input Machining Parameters on Cutting Forces

The ANOVA analysis is carried out at a confidence level of 95% (i.e., 5% significance level). Tables A2–A4 show the results of the ANOVA analysis. The regression models of cutting forces F_x , F_y , F_z with R^2 equal to 89.96, 94.21, 98.17, respectively, are given below in Equations (1)–(3).

$$F_x = -1422 - 18.9X_1 + 4.52X_2 + 44.1X_3 + 9.48X_1 * X_1 - 0.0232X_2 * X_2 - 0.383X_3 * X_3 \quad (1)$$

$$F_y = -2248 - 160.4X_1 + 25.03X_2 + 133.1X_3 + 71.7X_1 * X_1 - 0.1232X_2 * X_2 - 1.198X_3 * X_3 \quad (2)$$

$$F_z = -2403 - 158.0X_1 + 10.0X_2 + 73.2X_3 + 70.6X_1 * X_1 - 0.0519X_2 * X_2 - 0.621X_3 * X_3 \quad (3)$$

The Pareto charts of the standardized effects with $\alpha = 0.05$ for the response parameters F_x , F_y , F_z are shown in Figures 3–5. Hardness (x_3) has the strongest influence on F_x , F_z , while nanoparticle concentration (x_1) has a strongest influence on F_y and also causes strong effect on F_z . It can be seen that cutting speed (x_2) has a very little effect on cutting forces F_x , F_y , F_z .

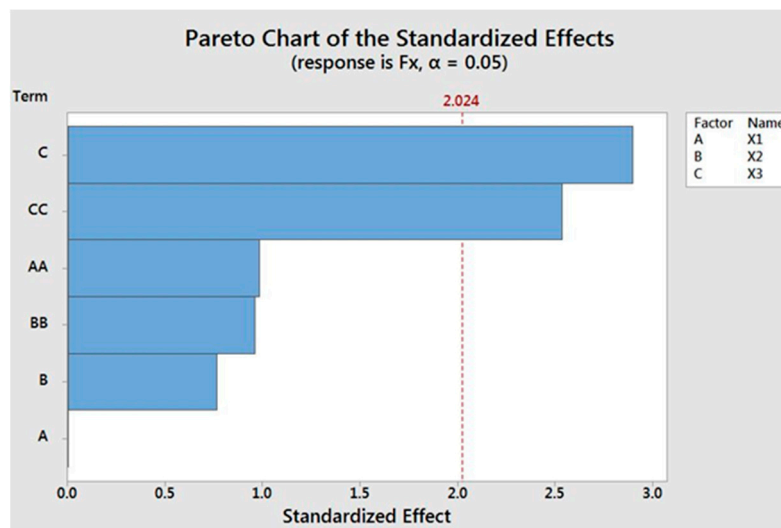


Figure 3. Pareto chart of effects of investigated factors on cutting force F_x . (A is x_1 : nanoparticle concentration, B is x_2 : cutting speed, C is x_3 : hardness, AA is the quadratic effect of nanoparticle concentration, BB is the quadratic effect of cutting speed, and CC is the quadratic effect of hardness).

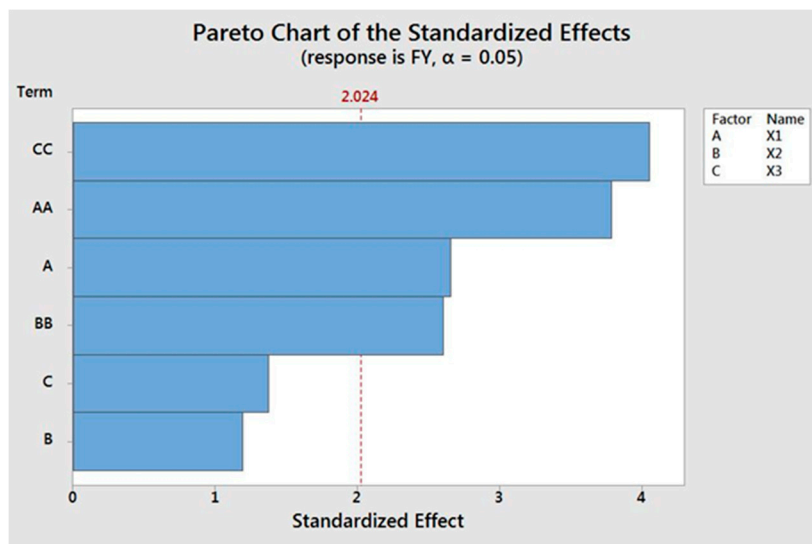


Figure 4. Pareto chart of effects of investigated factors on cutting force F_y . (A is x_1 : nanoparticle concentration, B is x_2 : cutting speed, C is x_3 : hardness, AA is the quadratic effect of nanoparticle concentration, BB is the quadratic effect of cutting speed, and CC is the quadratic effect of hardness).

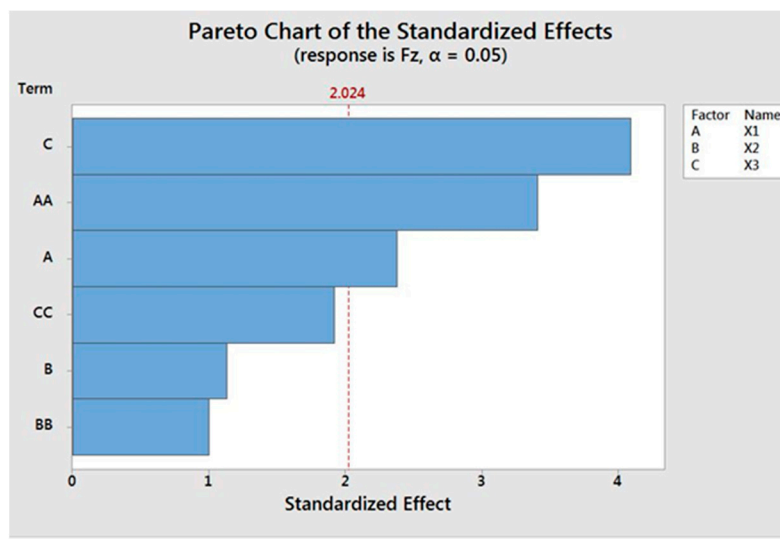


Figure 5. Pareto chart of effects of investigated factors on cutting force F_z . (A is x_1 : nanoparticle concentration, B is x_2 : cutting speed, C is x_3 : hardness, AA is the quadratic effect of nanoparticle concentration, BB is the quadratic effect of cutting speed, and CC is the quadratic effect of hardness).

The quadratic effect CC (x_3x_3) reveals the significant influence on the investigated functions of F_x , F_y , and the quadratic effect AA (x_1x_1) exhibits the significant effect on the investigated functions of F_y , F_z . In addition, the quadratic effect BB (x_2x_2) has a strong influence on F_y . The other quadratic effects of x_1x_2 , x_1x_3 , x_2x_3 cause very little influences and are not investigated in the regression models. Studying the charts in Figures 3–5, the proper selection of nanoparticle concentration and hardness is needed to study for the effects on cutting forces in order to improve the machining performance while retaining the good tool life and surface quality as well.

The surface and contour plots of investigated variables on cutting force F_x are shown in Figures 6–8.

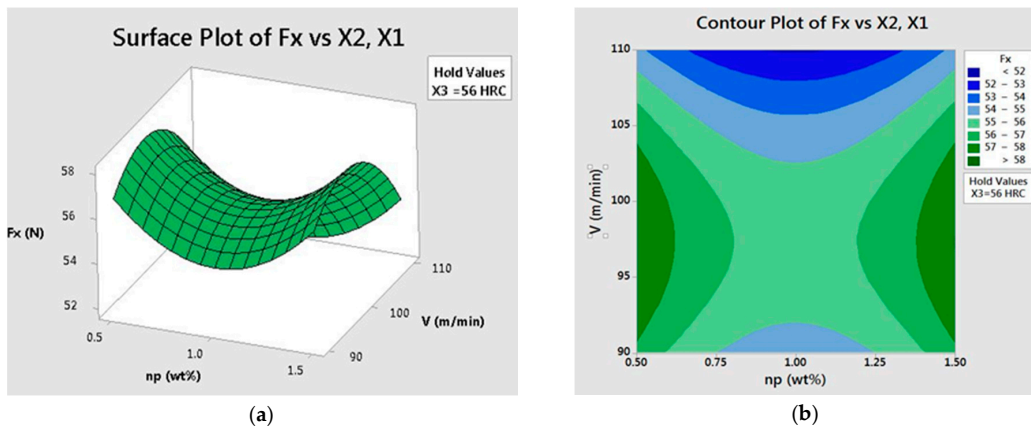


Figure 6. Effects of nanoparticle concentration and cutting speed on cutting force F_x : (a) surface plot, (b) contour plot.

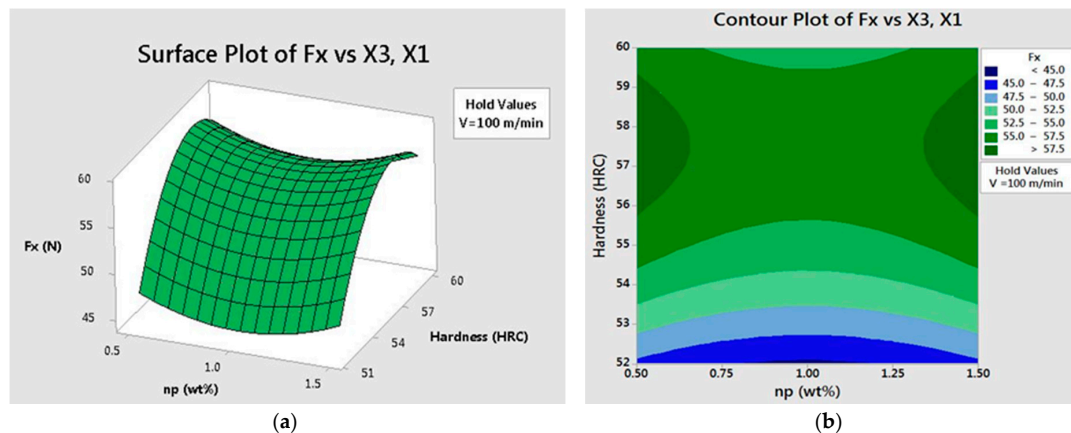


Figure 7. Effects of nanoparticle concentration and hardness on cutting force F_x : (a) surface plot, (b) contour plot.

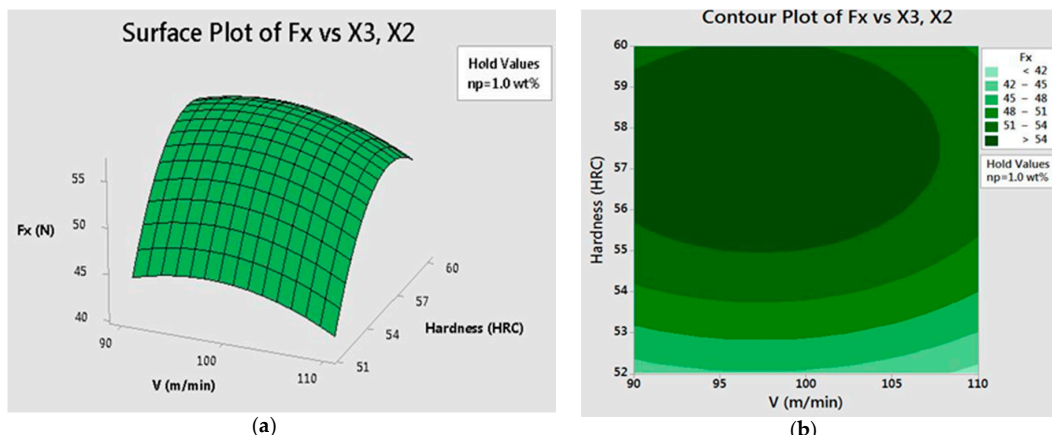


Figure 8. Effects of cutting speed and hardness on cutting force F_x : (a) surface plot, (b) contour plot.

The graphs of effects of nanoparticle concentration and cutting speed with constant hardness of 56 HRC are shown in Figure 6. From Figure 6a, the cutting force F_x increases with the rise of cutting speed from 90 to 100 m/min and then decreases when cutting speed rises to 110 m/min, but the surface plot is contrast with the changes of nanoparticle concentration. Observed from Figure 6b, the aim for low cutting force F_x can achieve by using high level of cutting speed (110 m/min) and np of 1.0 wt.%. When holding cutting speed of 100 m/min or nanoparticle concentration of 1.0 wt.%, it can be clearly

seen that the hardness factor has a very strong effect on cutting forces F_x (Figures 7 and 8). The force F_x rapidly goes up with the rise of material hardness.

The surface and contour plots of nanoparticle concentration and cutting speed on cutting forces F_y, F_z while keeping the constant hardness of 56HRC are shown in Figures 9 and 10.

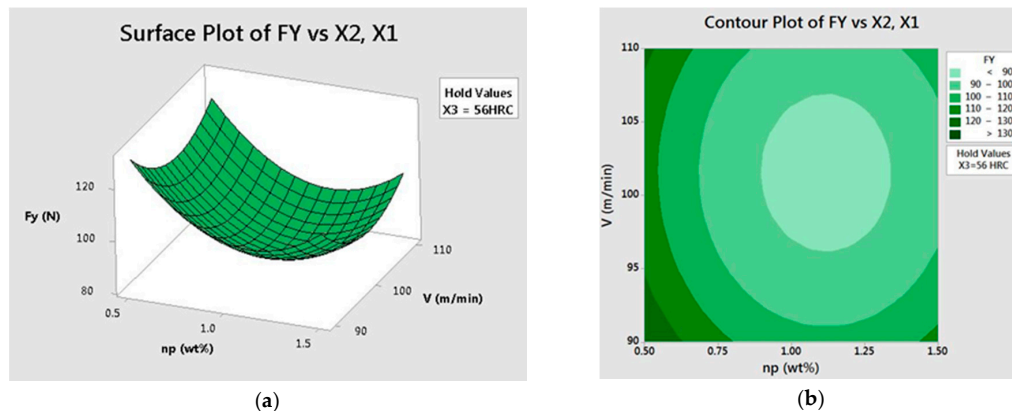


Figure 9. Effects of nanoparticle concentration and cutting speed on cutting force F_y : (a) surface plot, (b) contour plot.

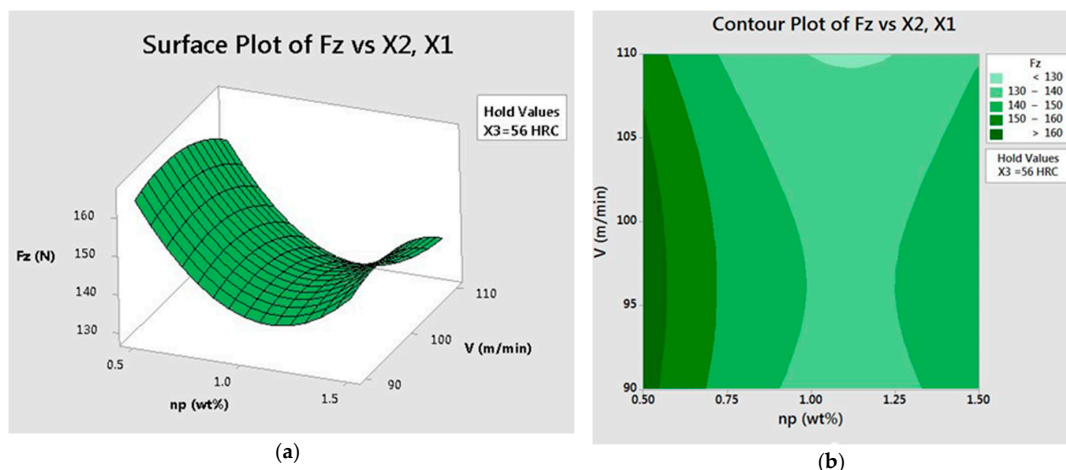


Figure 10. Effects of nanoparticle concentration and cutting speed on cutting force F_z : (a) surface plot, (b) contour plot.

From the surface and contour plots in Figures 9 and 10, it clearly reveals that the value of nanoparticle concentration of 1.0 wt.% brings out the decrease of cutting forces F_y, F_z . For smallest values of F_y , cutting speed can be chosen from 95 to 105 m/min (Figure 9b), and for smallest values of F_z , it can range from 90 to 110 m/min (Figure 10b). Hence, depending on the specific conditions, these results could provide the useful guide for improving hard milling performance while ensuring the technical and economic characteristics.

The surface and contour plots of hardness and nanoparticle concentration on cutting forces F_y, F_z while cutting speed is constant with $V = 100$ m/min are shown in Figures 11 and 12.

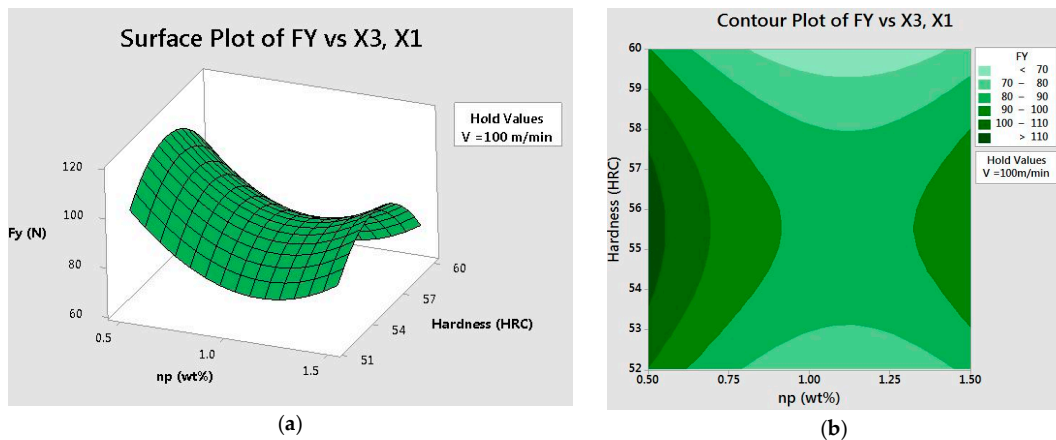


Figure 11. Effects of nanoparticle concentration and hardness on cutting force F_y : (a) surface plot, (b) contour plot.

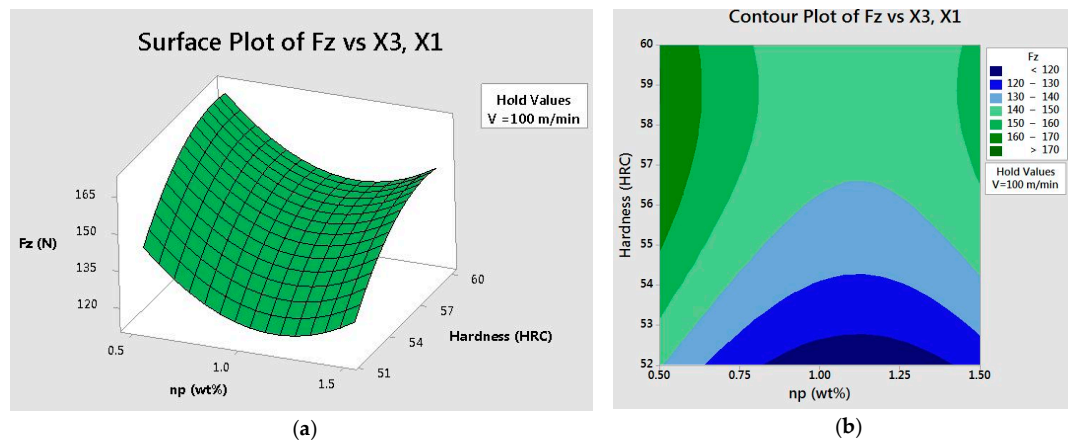


Figure 12. Effects of nanoparticle concentration and hardness on cutting force F_z : (a) surface plot, (b) contour plot.

From the surface and contour plots in Figures 11 and 12, it clearly reveals that the value of nanoparticle concentration about 1.0 wt.% also gives out the decrease of cutting forces F_y , F_z . The cutting forces F_y , F_z grow with the increase of material hardness from 52 to 56 HRC, but there is a little difference in the hardness range of 56–60 HRC. The force F_y exhibits the reducing trend while the force F_z increases.

The surface and contour plots of hardness and cutting speed on cutting forces F_y , F_z while nanoparticle concentration is constant with $np = 1.0$ wt.% are shown in Figures 13 and 14. In general, when cutting speed increases, the forces F_y , F_z decrease but not much. From these results, nanoparticle concentration can be chosen by about 1.0 wt.% in combination with a low hardness value, and a high cutting speed can be used for increasing productivity.

In detail, F_y is the thrust force, the so-called springback of the work materials, which plays a significant role in hard machining and has a strong effect dimensional accuracy and flank wear. Moreover, it causes high contact stresses over the tool flank contact face and this is a distinguishing feature of hard machining. F_z is the main cutting force, which has a strong effect on the cutting performance and productivity. From the study, the technical guides will be given for selecting the cutting condition and making further studies.

In the machining of hardened steels with geometrically defined cutting tools, catastrophic failure causes the saw-tooth chip formation in the primary shear zone. Thermal stresses originate mainly in the intensive friction between the flank face and machined face. Moreover, the plastic deformation is very little, so the thermal stresses and intensive friction cause white layer [2]. Therefore, the presence

of MoS₂ nanosheet having a low friction coefficient and excellent lubricating property in MQCL-based fluid contributes to reducing the friction stresses in contact zones [38,39], from which the cutting forces decrease significantly and the machining performance improves.

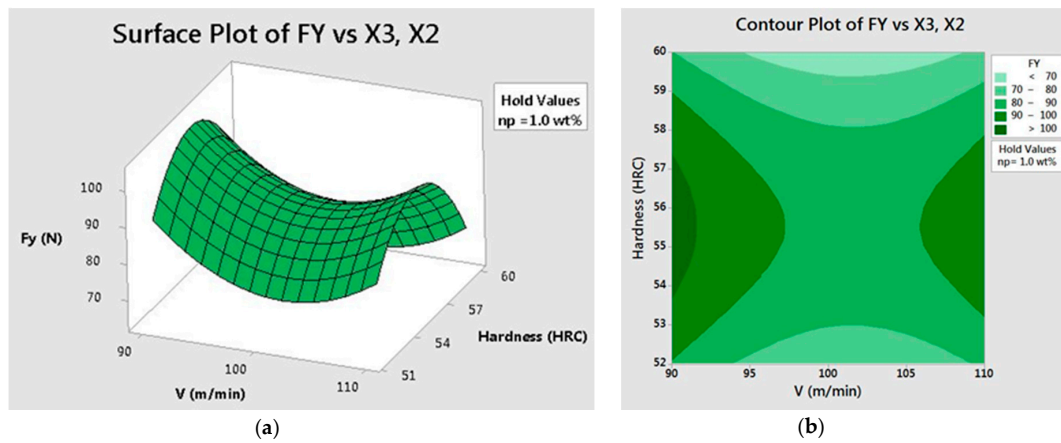


Figure 13. Effects of cutting speed and hardness on cutting force F_y : (a) surface plot, (b) contour plot.

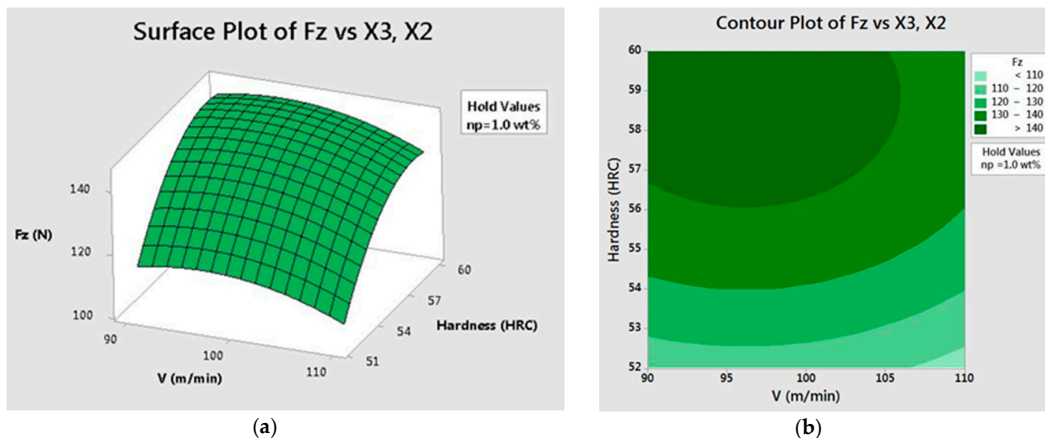


Figure 14. Effects of cutting speed and hardness on cutting force F_z : (a) surface plot, (b) contour plot.

4. Conclusions

In this study, MoS₂ nanoparticles are produced by exfoliation of liquid N₂-quenched bulk, which is the facile method owing to its highly efficient, green, and facile operation. The produced MoS₂ nanosheets are directly used for the MQCL hard milling process. Box-Behnken experimental design with the help of ANOVA analysis is used to investigate the effects of three variables, including nanoparticle concentration, cutting speed, and material hardness on cutting force components F_x , F_y , F_z .

From the obtained results, hardness and nanoparticle concentration reveal the strongest influence on the cutting force functions. The nanoparticle concentration should be used with 1.0 wt.% for reducing cutting forces in combination with a high cutting speed of 110 m/min in order to achieve the technological and economic characteristics. The cutting force components grow up with the increase of hardness.

The machining performance of hard milling process improves under the MQCL condition by using an MQCL device named the Frigid-X Sub-Zero Vortex Tool Cooling Mist System with a real cooling effect based on the principle of the Ranque–Hilsch vortex tube. The cooling and lubricating effects significantly enhance due to the use of the novel MQCL device and MoS₂ nanofluid with excellent lubricating property. Therefore, the normal coated cemented carbide inserts, such as APMT 1604 PDTR LT30, could be effectively used for the hard machining of AISI D2 (52–60 HRC) with a high cutting

speed of 110 m/min, which is about 2.0–2.2 times higher than the manufacturer's recommendations [40]. This will contribute to enlarge the cutting applicability and decrease the manufacturing cost.

Moreover, this is one of the first studies of this type of MQCL tool using nanofluid for difficult-to-cut materials. Compared to our previous study, which concentrated on the surface roughness, surface microstructure, and surface profile and used the commercial MoS₂ nanoparticles [17], this work is a big development because MoS₂ nanoparticles are produced by our own method and cutting forces F_x, F_y, F_z are investigated in detail, from which the technical guides are provided and further work can be made.

Furthermore, the MQCL tool only needs ordinary air rather than cryogenic CO₂ or N₂ for cooling, which will simplify the equipment and reduce the cost.

In further research, deeper studies are needed to focus on the effects of MoS₂ nanoparticles on tool wear and tool life as well as the lubricating behavior in the cutting zone. In addition to this, the morphology, size and production methods of MoS₂ nanosheets will be investigated.

Author Contributions: Conceptualization, P.Q.D., T.M.D., T.T.L. and D.V.T.; Data curation, N.M.T.; Formal analysis, P.Q.D., T.T.L., D.V.T., N.M.T. and N.V.T.; Investigation, P.Q.D., T.T.L., N.M.T. and N.V.T.; Methodology, P.Q.D., T.T.L., D.V.T., N.M.T. and N.V.T.; Project administration, T.M.D.; Resources, D.V.T.; Software, T.T.L., D.V.T. and N.V.T.; Supervision, N.V.T.; Validation, N.M.T.; Visualization, T.T.L.; Writing—original draft, P.Q.D., T.M.D., T.T.L. and D.V.T.; Writing—review & editing, P.Q.D., T.M.D., T.T.L. and D.V.T. All authors have read and agreed to the published version of the manuscript.

Funding: This research was funded by Vietnam Ministry of Education and Training with the project number of B2019-TNA-02.

Acknowledgments: The study had the support of Vietnam Ministry of Education and Training and Thai Nguyen University of Technology, Thai Nguyen University with the project number of B2019-TNA-02.

Conflicts of Interest: The authors declare no conflict of interest.

Appendix A

Table A1. Design of the experiment with test run order and output in terms of cutting forces.

Std Order	Run Order	PtType	Blocks	Input Machining Parameters			Response Variables		
				x ₁ (wt.%)	x ₂ (m/min)	x ₃ (HRC)	F _x (N)	F _y (N)	F _z (N)
1	20	2	1	0.5	90	56	60.50	116.70	179.90
2	30	2	1	1.5	90	56	62.70	101.30	135.70
3	7	2	1	0.5	110	56	43.70	99.80	131.83
4	41	2	1	1.5	110	56	53.10	90.08	136.40
5	4	2	1	0.5	100	52	45.40	125.24	157.80
6	39	2	1	1.5	100	52	47.90	103.10	129.80
7	32	2	1	0.5	100	60	52.60	73.20	120.48
8	14	2	1	1.5	100	60	45.77	69.90	137.90
9	16	2	1	1	90	52	41.40	90.70	98.37
10	29	2	1	1	110	52	37.45	82.60	97.70
11	22	2	1	1	90	60	72.20	86.30	168.90
12	18	2	1	1	110	60	45.04	76.90	149.53
13	23	0	1	1	100	56	57.40	90.10	140.85
14	43	0	1	1	100	56	50.00	77.90	134.94
15	19	0	1	1	100	56	53.70	83.95	137.90
16	11	2	1	0.5	90	56	61.50	170.10	178.70
17	21	2	1	1.5	90	56	50.40	103.10	136.00
18	13	2	1	0.5	110	56	55.40	120.96	173.52
19	37	2	1	1.5	110	56	52.20	100.20	142.79
20	38	2	1	0.5	100	52	42.80	79.70	151.65

Table A1. Cont.

Std Order	Run Order	PtType	Blocks	Input Machining Parameters			Response Variables		
				x_1 (wt.%)	x_2 (m/min)	x_3 (HRC)	F_x (N)	F_y (N)	F_z (N)
21	33	2	1	1.5	100	52	52.40	105.10	145.79
22	12	2	1	0.5	100	60	54.30	80.45	154.08
23	9	2	1	1.5	100	60	62.59	87.80	171.50
24	28	2	1	1	90	52	43.10	83.96	92.85
25	45	2	1	1	110	52	47.60	99.50	112.40
26	10	2	1	1	90	60	40.40	68.53	141.90
27	2	2	1	1	110	60	37.30	80.83	134.87
28	15	0	1	1	100	56	65.70	94.90	145.03
29	36	0	1	1	100	56	50.40	84.60	130.40
30	27	0	1	1	100	56	58.05	89.75	137.50
31	6	2	1	0.5	90	56	46.20	151.90	160.10
32	17	2	1	1.5	90	56	58.60	102.50	138.70
33	5	2	1	0.5	110	56	58.60	124.90	163.76
34	3	2	1	1.5	110	56	56.40	114.70	140.28
35	35	2	1	0.5	100	52	43.50	65.80	112.00
36	25	2	1	1.5	100	52	52.60	77.00	141.55
37	42	2	1	0.5	100	60	61.90	90.95	145.90
38	1	2	1	1.5	100	60	48.90	70.10	132.25
39	31	2	1	1	90	52	40.77	87.90	126.20
40	26	2	1	1	110	52	40.50	57.20	84.78
41	8	2	1	1	90	60	52.60	76.70	142.50
42	40	2	1	1	110	60	66.00	80.06	136.51
43	44	0	1	1	100	56	64.60	94.80	142.85
44	24	0	1	1	100	56	44.76	84.39	140.22
45	34	0	1	1	100	56	54.68	89.60	141.37

Table A2. Results of the ANOVA analysis of cutting force F_x .

Source	DF	Adj SS	Adj MS	F-Value	p-Value
Model	6	1133.64	188.941	2.93	0.019
Linear	3	580.91	193.638	3.00	0.042
x_1	1	0.00	0.001	0.00	0.997
x_2	1	37.70	37.700	0.58	0.449
x_3	1	543.21	543.211	8.42	0.006
Square	3	552.73	184.244	2.85	0.050
$x_1^*x_1$	1	62.22	62.218	0.96	0.332
$x_2^*x_2$	1	59.71	59.706	0.93	0.342
$x_3^*x_3$	1	415.56	415.558	6.44	0.015
Error	38	2452.38	64.536		
Lack-of-Fit	6	185.94	30.989	0.44	0.848
Pure Error	32	2266.45	70.827		
Total	44	3586.03			

* represents the quadratic effect.

Table A3. Results of the ANOVA analysis of cutting force F_y .

Source	DF	Adj SS	Adj MS	F-Value	p-Value
Model	6	12,556.1	2092.7	8.47	0.000
Linear	3	2569.2	856.4	3.47	0.025
x_1	1	1748.0	1748.0	7.07	0.011
x_2	1	352.4	352.4	1.43	0.240
x_3	1	468.9	468.9	1.90	0.176
Square	3	9986.9	3329.0	13.47	0.000
$x_1^*x_1$	1	3557.1	3557.1	14.39	0.001
$x_2^*x_2$	1	1682.2	1682.2	6.81	0.013
$x_3^*x_3$	1	4069.9	4069.9	16.47	0.000
Error	38	9391.8	247.2		
Lack-of-Fit	6	2198.1	366.4	1.63	0.171
Pure Error	32	7193.7	224.8		
Total	44	21,947.9			

* represents the quadratic effect.

Table A4. Results of the ANOVA analysis of cutting force F_z .

Source	DF	Adj SS	Adj MS	F-Value	p-Value
Model	6	12,281.2	2046.9	6.91	0.000
Linear	3	7035.7	2345.2	7.91	0.000
x_1	1	1684.4	1684.4	5.68	0.022
x_2	1	379.6	379.6	1.28	0.265
x_3	1	4971.7	4971.7	16.78	0.000
Square	3	5245.4	1748.5	5.90	0.002
$x_1^*x_1$	1	3453.8	3453.8	11.66	0.002
$x_2^*x_2$	1	298.5	298.5	1.01	0.322
$x_3^*x_3$	1	1094.3	1094.3	3.69	0.062
Error	38	11,259.9	296.3		
Lack-of-Fit	6	2278.0	379.7	1.35	0.263
Pure Error	32	8981.9	280.7		
Total	44	23,541.1			

* represents the quadratic effect.

References

1. Nagimova, A.; Perveen, A. A review on Laser Machining of hard to cut materials. *Mater. Today Proc.* **2019**, *18*, 2440–2447. [[CrossRef](#)]
2. Davim, J.P. *Machining of Hard Materials*; Springer: London, UK, 2011.
3. Zhang, K.; Deng, J.; Meng, R.; Gao, P.; Yue, H. Effect of nano-scale textures on cutting performance of WC/Co-based Ti55Al45N coated tools in dry cutting. *Int. J. Refract. Met. Hard Mater.* **2015**, *51*, 35–49. [[CrossRef](#)]
4. Xing, Y.; Deng, J.; Zhao, J.; Zhang, G.; Zhang, K. Cutting performance and wear mechanism of nanoscale and microscale textured Al₂O₃/TiC ceramic tools in dry cutting of hardened steel. *Int. J. Refract. Met. Hard Mater.* **2014**, *43*, 46–58. [[CrossRef](#)]

5. Bouacha, K.; Yallese, M.A.; Mabrouki, T.; Rigal, J.-F. Statistical analysis of surface roughness and cutting forces using response surface methodology in hard turning of AISI 52100 bearing steel with CBN tool. *Int. J. Refract. Met. Hard Mater.* **2010**, *28*, 349–361. [[CrossRef](#)]
6. Su, Y.; Li, Z.; Li, L.; Wang, J.; Gao, H.; Wang, G. Cutting performance of micro-textured polycrystalline diamond tool in dry cutting. *J. Manuf. Process.* **2017**, *27*, 1–7. [[CrossRef](#)]
7. Vignesh, M.; Ramanujam, R. *Laser-assisted high Speed Machining of Inconel 718 Alloy*; Elsevier BV: Amsterdam, The Netherlands, 2020; pp. 243–262.
8. Venkatesan, K. Optimization of Surface Roughness and Power Consumption in laser-assisted machining of Inconel 718 by Taguchi based Response Surface Methodology. *Mater. Today Proc.* **2018**, *5*, 11326–11335. [[CrossRef](#)]
9. Duc, M.T.; Long, T.T. Investigation of MQL-Employed Hard-Milling Process of S60C Steel Using Coated-Cemented Carbide Tools. *J. Mech. Eng. Autom.* **2016**, *6*, 128–132.
10. Joshi, K.K.; Kumar, R. Anurag An Experimental Investigations in Turning of Incoloy 800 in Dry, MQL and Flood Cooling Conditions. *Procedia Manuf.* **2018**, *20*, 350–357. [[CrossRef](#)]
11. Sani, A.S.A.; Rahim, E.A.; Sharif, S.; Sasahara, H. Machining performance of vegetable oil with phosphonium- and ammonium-based ionic liquids via MQL technique. *J. Clean. Prod.* **2019**, *209*, 947–964. [[CrossRef](#)]
12. Minh, D.T.; The, L.T.; Bao, N.T. Performance of Al₂O₃ nanofluids in minimum quantity lubrication in hard milling of 60Si₂Mn steel using cemented carbide tools. *Adv. Mech. Eng.* **2017**, *9*, 1–9. [[CrossRef](#)]
13. Hegab, H.; Umer, U.; Soliman, M.; Kishawy, H.A. Effects of nano-cutting fluids on tool performance and chip morphology during machining Inconel 718. *Int. J. Adv. Manuf. Technol.* **2018**, *96*, 3449–3458. [[CrossRef](#)]
14. Hegab, H.; Kishawy, H.A. Towards Sustainable Machining of Inconel 718 Using Nano-Fluid Minimum Quantity Lubrication. *J. Manuf. Mater. Process.* **2018**, *2*, 50. [[CrossRef](#)]
15. Tran, M.-D.; Long, T.T.; Chien, T.Q. Performance Evaluation of MQL Parameters Using Al₂O₃ and MoS₂ Nanofluids in Hard Turning 90CrSi Steel. *Lubricants* **2019**, *7*, 40. [[CrossRef](#)]
16. Duc, T.M.; Long, T.T.; Dong, P.Q. Effect of the alumina nanofluid concentration on minimum quantity lubrication hard machining for sustainable production. *Proc. Inst. Mech. Eng. Part C J. Mech. Eng. Sci.* **2019**, *233*, 5977–5988. [[CrossRef](#)]
17. Dong, P.Q.; Duc, T.M.; Long, T.T. Performance Evaluation of MQCL Hard Milling of SKD 11 Tool Steel Using MoS₂ Nanofluid. *Metals* **2019**, *9*, 658. [[CrossRef](#)]
18. Li, B.; Li, C.; Zhang, Y.; Wang, Y.; Jia, D.; Yang, M.; Zhang, Y.; Wu, Q.; Han, Z.; Sun, K. Heat transfer performance of MQL grinding with different nanofluids for Ni-based alloys using vegetable oil. *J. Clean. Prod.* **2017**, *154*, 1–11. [[CrossRef](#)]
19. Pashmforoush, F.; Bagherinia, R.D. Influence of water-based copper nanofluid on wheel loading and surface roughness during grinding of Inconel 738 superalloy. *J. Clean. Prod.* **2018**, *178*, 363–372. [[CrossRef](#)]
20. Lee, P.-H.; Nam, J.S.; Li, C.; Lee, S.W. An experimental study on micro-grinding process with nanofluid minimum quantity lubrication (MQL). *Int. J. Precis. Eng. Manuf.* **2012**, *13*, 331–338. [[CrossRef](#)]
21. Zhang, Y.; Li, C.; Jia, D.; Li, B.; Wang, Y.; Yang, M.; Hou, Y.; Zhang, X. Experimental study on the effect of nanoparticle concentration on the lubricating property of nanofluids for MQL grinding of Ni-based alloy. *J. Mater. Process. Technol.* **2016**, *232*, 100–115. [[CrossRef](#)]
22. Yıldırım, Ç.V.; Sarıkaya, M.; Kivak, T.; Şirin, Ş. The effect of addition of hBN nanoparticles to nanofluid-MQL on tool wear patterns, tool life, roughness and temperature in turning of Ni-based Inconel 625. *Tribol. Int.* **2019**, *134*, 443–456. [[CrossRef](#)]
23. Yıldırım, Ç.V. Investigation of hard turning performance of eco-friendly cooling strategies: Cryogenic cooling and nanofluid based MQL. *Tribol. Int.* **2020**, *144*, 106127. [[CrossRef](#)]
24. Pervaiz, S.; Deiab, I.; Rashid, A.; Nicolescu, M. Minimal quantity cooling lubrication in turning of Ti6Al4V: Influence on surface roughness, cutting force and tool wear. *Proc. Inst. Mech. Eng. Part B J. Eng. Manuf.* **2015**, *231*, 1542–1558. [[CrossRef](#)]
25. Maruda, R.W.; Krolczyk, G.M.; Feldshtein, E.; Nieslony, P.; Tyliszczak, B.; Pusavec, F. Tool wear characterizations in finish turning of AISI 1045 carbon steel for MQCL conditions. *Wear* **2017**, *372*, 54–67. [[CrossRef](#)]
26. Maruda, R.W.; Krolczyk, G.M.; Feldshtein, E.; Pusavec, F.; Szydlowski, M.; Legutko, S.; Sobczak-Kupiec, A. A study on droplets sizes, their distribution and heat exchange for minimum quantity cooling lubrication (MQCL). *Int. J. Mach. Tools Manuf.* **2016**, *100*, 81–92. [[CrossRef](#)]

27. Maruda, R.W.; Krolczyk, G.M.; Nieslony, P.; Królczyk, J.B.; Legutko, S. Chip Formation Zone Analysis During the Turning of Austenitic Stainless Steel 316L under MQCL Cooling Condition. *Procedia Eng.* **2016**, *149*, 297–304. [CrossRef]
28. Maruda, R.W.; Feldshtein, E.; Legutko, S.; Królczyk, G.M. Research on emulsion mist generation in the conditions of minimum quantity cooling lubrication (MQCL). *Teh. Vjesn. Tech. Gaz.* **2015**, *22*, 1213–1218. [CrossRef]
29. Duc, T.M.; Long, T.T.; Van Thanh, D. Evaluation of minimum quantity lubrication and minimum quantity cooling lubrication performance in hard drilling of Hardox 500 steel using Al_2O_3 nanofluid. *Adv. Mech. Eng.* **2020**, *12*, 1–12. [CrossRef]
30. Zeng, Z.; Yin, Z.; Huang, X.; Li, H.; He, Q.; Lu, G.; Boey, F.; Zhang, H. Single-Layer Semiconducting Nanosheets: High-Yield Preparation and Device Fabrication. *Angew. Chem. Int. Ed.* **2011**, *50*, 11093–11097. [CrossRef]
31. Lee, Y.-H.; Zhang, X.; Zhang, W.; Chang, M.-T.; Lin, C.-T.; Chang, K.-D.; Yu, Y.-C.; Wang, J.T.-W.; Chang, C.-S.; Li, L.-J.; et al. Synthesis of Large-Area MoS_2 Atomic Layers with Chemical Vapor Deposition. *Adv. Mater.* **2012**, *24*, 2320–2325. [CrossRef]
32. Liu, K.-K.; Zhang, W.; Lee, Y.-H.; Lin, Y.-C.; Chang, M.-T.; Su, C.Y.; Chang, C.-S.; Li, H.; Shi, Y.; Zhang, H.; et al. Growth of Large-Area and Highly Crystalline MoS_2 Thin Layers on Insulating Substrates. *Nano Lett.* **2012**, *12*, 1538–1544. [CrossRef]
33. Yu, Y.; Li, C.; Liu, Y.; Su, L.; Zhang, Y.; Cao, L. Controlled Scalable Synthesis of Uniform, High-Quality Monolayer and Few-layer MoS_2 Films. *Sci. Rep.* **2013**, *3*, 1866. [CrossRef] [PubMed]
34. Wu, S.; Huang, C.; Aivazian, G.; Ross, J.S.; Cobden, D.H.; Xu, X. Vapor–Solid Growth of High Optical Quality MoS_2 Monolayers with Near-Unity Valley Polarization. *ACS Nano* **2013**, *7*, 2768–2772. [CrossRef] [PubMed]
35. Van Thanh, D.; Pan, C.-C.; Chu, C.-W.; Wei, K.-H. Production of few-layer MoS_2 nanosheets through exfoliation of liquid N_2 -quenched bulk MoS_2 . *RSC Adv.* **2014**, *4*, 15586–15589. [CrossRef]
36. Nguyen, V.-T.; Yang, T.-Y.; Le, P.A.; Yen, P.-J.; Chueh, Y.-L.; Wei, K.-H. New Simultaneous Exfoliation and Doping Process for Generating MX_2 Nanosheets for Electrocatalytic Hydrogen Evolution Reaction. *ACS Appl. Mater. Interfaces* **2019**, *11*, 14786–14795. [CrossRef]
37. Nguyen, V.-T.; Le, P.A.; Hsu, Y.-C.; Wei, K.-H. Plasma-Induced Exfoliation Provides Onion-Like Graphene-Surrounded MoS_2 Nanosheets for a Highly Efficient Hydrogen Evolution Reaction. *ACS Appl. Mater. Interfaces* **2020**, *12*, 11533–11542. [CrossRef]
38. Rahmati, B.; Sarhan, A.A.; Sayuti, M. Morphology of surface generated by end milling AL6061-T6 using molybdenum disulfide (MoS_2) nanolubrication in end milling machining. *J. Clean. Prod.* **2014**, *66*, 685–691. [CrossRef]
39. Maruda, R.W.; Krolczyk, G.M.; Wojciechowski, S.; Źak, K.; Habrat, W.; Nieslony, P. Effects of extreme pressure and anti-wear additives on surface topography and tool wear during MQCL turning of AISI 1045 steel. *J. Mech. Sci. Technol.* **2018**, *32*, 1585–1591. [CrossRef]
40. Applied Research of Nanofluids in MQL to Improve Hard Milling Performance of $60\text{Si}_2\text{Mn}$ Steel Using Carbide Tools. Available online: <https://wix.laminatech.ch/img/catalog/1237.pdf> (accessed on 5 June 2019).



© 2020 by the authors. Licensee MDPI, Basel, Switzerland. This article is an open access article distributed under the terms and conditions of the Creative Commons Attribution (CC BY) license (<http://creativecommons.org/licenses/by/4.0/>).